Supercontinuum generation in silicon waveguides relying on wave-breaking

David Castelló-Lurbe[1,2*] **and Enrique Silvestre**[2]

[1]*Brussels Photonics Team (B-PHOT), Department of Applied Physics and Photonics (IR-TONA), Vrije Universiteit Brussel, Pleinlaan 2, B-1050 Brussels, Belgium*
[2]*Departament d'Òptica, Universitat de València, E-46100 Burjassot, Spain*
[*]*david.castello-lurbe@vub.ac.be*

Abstract: Four-wave-mixing processes enabled during optical wave-breaking (OWB) are exploited in this paper for supercontinuum generation. Unlike conventional approaches based on OWB, phase-matching is achieved here for these nonlinear interactions, and, consequently, new frequency production becomes more efficient. We take advantage of this kind of pulse propagation to obtain numerically a coherent octave-spanning mid-infrared supercontinuum generation in a silicon waveguide pumping at telecom wavelengths in the normal dispersion regime. This scheme shows a feasible path to overcome limits imposed by two-photon absorption on spectral broadening in silicon waveguides.

OCIS codes: (130.3120) Integrated optics devices; (190.4390) Nonlinear optics, integrated optics.

References and links

1. D. J. Jones, S. A. Diddams, J. K. Ranka, A. Stentz, R. S. Windeler, J. L. Hall, and S. T. Cundiff, "Carrier-envelope phase control of femtosecond mode-locked lasers and direct optical frequency synthesis," Science **288**, 635–639 (2000).
2. I. Hartl, X. D. Li, C. Chudoba, R. K. Ghanta, T. H. Ko, J. G. Fujimoto, J. K. Ranka and R. S. Windeler, "Ultrahigh-resolution optical coherence tomography using continuum generation in an airsilica microstructure optical fiber," Opt. Lett. **26**, 608–610 (2001).
3. S.V. Smirnov, J. D. Ania-Castanon, T. J. Ellingham, S. M. Kobtsev, S. Kukarin, S. K. Turitsyn, "Optical spectral broadening and supercontinuum generation in telecom applications," Opt. Fiber Technol. **12**, 122–147 (2006).
4. J. M. Dudley, G. Genty, and S. Coen, "Supercontinuum generation in photonic crystal fiber," Rev. Mod. Phys. **78**, 1135–1184 (2006).
5. A. V. Husakou and J. Herrmann, "Supercontinuum generation of higher-order solitons by fission in photonic crystal fibers," Phys. Rev. Lett. **27**, 203901 (2001).
6. G. Genty, S. Coen, and J. M. Dudley, "Fiber supercontinuum sources," J. Opt. Soc. Am. B **24**, 1771–1785 (2007).
7. M. Nakazawa, K. Tamura, H. Kubota, and E. Yoshida, "Coherence degradation in the process of supercontinuum generation in an optical fiber," Opt. Fiber Technol. **4**, 215–223 (1998).
8. Y. Takushima, and K. Kikuchi, "10-GHz, over 20-channel multiwavelength pulse source by slicing super-continuum spectrum generated in normal-dispersion-fiber," IEEE Photon. Technol. Lett. **11**, 322–324 (1999).
9. C. Finot, B. Kibler, L. Provost, and S. Wabnitz,"Beneficial impact of wave-breaking for coherent continuum formation in normally dispersive nonlinear fibers," J. Opt. Soc. Am. B **25**, 1938–1948 (2008).
10. J. J. Miret, E. Silvestre, and P. Andrés, "Octave-spanning ultraflat supercontinuum with soft-glass photonic crystal fibers," Opt. Express **17**, 9197–9203 (2009).
11. A. M. Heidt, A. Hartung, G. W. Bosman, P. Krok, E. G. Rohwer, H. Schwoerer, and H. Bartelt,"Coherent octave spanning near-infrared and visible supercontinuum generation in all-normal dispersion photonic crystal fibers," Opt. Express **19**, 3775–3787 (2011).
12. W. J. Tomlinson, R. H. Stolen, and A. M. Johnson, "Optical wave-breaking in nonlinear optical fibers," Opt. Lett. **10**, 457-459 (1985).
13. J. E. Rothenberg and D. Grischkowsky, "Observation of the formation of an optical intensity shock and wave breaking in the nonlinear propagation of pulses in optical fibers," Phys. Rev. Lett. **62**, 531–534 (1989).

14. J. E. Rothenberg, "Femtosecond optical shocks and wave breaking in fiber propagation," J. Opt. Soc. Am. B **6**, 2392–2401 (1989).
15. J. Wu, F. Luo, Q. Zhang, and M. Cao, "Optical wave breaking of high-intensity femtosecond pulses in silicon optical waveguides," Opt. Laser Technol. **41**, 360–364 (2009).
16. Y. Liu, H. Tu, and S. A. Boppart, "Wave-breaking-extended fiber supercontinuum generation for high compression ratio transform-limited pulse compression," Opt. Lett. **37**, 2172-2174 (2012).
17. K. E. Webb, Y. Q. Xu, M. Erkintalo, and S. G. Murdoch, "Generalized dispersive wave emission in nonlinear fibers," Opt. Lett. **38**, 151–153 (2013).
18. M. Erkintalo, Y. Q. Xu, S. G. Murdoch, J. M. Dudley, and G. Genty, "Cascaded phase matching and nonlinear symmetry breaking in fiber frequency combs," Phys. Rev. Lett. **109**, 223904 (2012).
19. M. Conforti and S. Trillo, "Dispersive wave emission from wave breaking," Opt. Lett. **38**, 3815–3818 (2013).
20. D. Castelló-Lurbe, P. Andrés, and E. Silvestre, "Dispersion-to-spectrum mapping in nonlinear fibers based on optical wave-breaking," Opt. Express **21**, 28550–28558 (2013).
21. B. Jalali and S. Fathpour, "Silicon Photonics," J. Lightwave Technol. **24**, 4600–4615 (2006).
22. M. Dinu, F. Quochi, and H. Garcia, "Third-order nonlinearities in silicon at telecom wavelengths," Appl. Phys. Lett. **82**, 2954 (2003).
23. Q. Lin, J. Zhang, G. Piredda, R. W. Boyd, P. M. Fauchet, and G. P. Agrawal, "Dispersion of silicon nonlinearities in the near infrared region," Appl. Phys. Lett. **91**, 021111 (2007).
24. A. D. Bristow, N. Rotenberg, and H. M. van Driel, "Two-photon absorption and Kerr coefficients of silicon for 850–2200 nm," Appl. Phys. Lett. **90**, 191104 (2007).
25. M. Lipson, "Guiding, modulating, and emitting light on silicon. Challenges and opportunities," J. Lightwave Technol. **23**, 4222–4238 (2005).
26. L. Yin and G. P. Agrawal, "Impact of two-photon absorption on self-phase modulation in silicon waveguides," Opt. Lett. **32**, 2031–2033 (2007).
27. P. Koonath, D. R. Solli, and B. Jalali, "Limiting nature of continuum generation in silicon," Appl. Phys. Lett. **93**, 091114 (2008).
28. Q. Lin, O. J. Painter, and G. P. Agrawal, "Nonlinear optical phenomena in silicon waveguides: Modeling and applications," Opt. Express **15**, 16604–16644 (2007).
29. R. M. Osgood, Jr., N. C. Panoiu, J. I. Dadap, X. Liu, X. Chen, I-W. Hsieh, E. Dulkeith, W. M. J. Green, and Y. A. Vlasov, "Engineering nonlinearities in nanoscale optical systems: physics and applications in dispersion-engineered silicon nanophotonic wires," Adv. Opt. Photon. **1**, 162–235 (2009).
30. D. Castelló-Lurbe, V. Torres-Company, and E. Silvestre, "Inverse dispersion engineering in silicon waveguides," J. Opt. Soc. Am. B **31**, 1829–1835 (2014).
31. Sh. Amiranashvili and A. Demircan, "Ultrashort Optical Pulse Propagation in terms of Analytic Signal," Adv. Opt. Technol. **2011**, 989515 (2011).
32. M. Conforti, A. Marini, T. X. Tran, D. Faccio, and F. Biancalana, "Interaction between optical fields and their conjugates in nonlinear media;" Opt. Express **21**, 31239–31252 (2013).
33. J. Lægsgaard, "Mode profile dispersion in the generalized nonlinear Schrödinger equation," Opt. Express **15**, 16110–16123 (2007).
34. B. Barviau, B. Kibler, and A. Picozzi, "Wave-turbulence approach of supercontinuum generation: influence of self-steepening and higher-order dispersion," Phys. Rev. A **79**, 063840 (2009).
35. C. Michel, P. Suret, S. Randoux, H. R. Jauslin, and A. Picozzi, "Influence of third-order dispersion on the propagation of incoherent light in optical fibers," Opt. Lett. **35**, 2367–2369 (2010).
36. G. P. Agrawal, *Nonlinear Fiber Optics* (Academic Press, 4th ed., 2007).
37. M. E. Marhic, N. Kagi, T.-K. Chiang, and L. G. Kazovsky, "Broadband fiber optical parametric amplifiers," Opt. Lett. **21**, 573–575 (1996).
38. N. Akhmediev and M. Karlsson, "Cherenkov radiation emitted by solitons in optical fibers," Phys. Rev. A **51**, 2602–20607 (1995).
39. M. Conforti, F. Baronio, and S. Trillo, "Resonant radiation shed by dispersive shock waves," Phys. Rev. A **89**, 013807 (2014).
40. D. Anderson, M. Desaix, M. Lisak, and M. L. Quiroga-Teixeiro,"Wave breaking in nonlinear-optical fibers," J. Opt. Soc. Am. B **9**, 1358–1361 (1992).
41. X. Liu, R. M. Osgood Jr, Y. A. Vlasov and W. M. J. Green, "Mid-infrared optical parametric amplifier using silicon nanophotonic waveguides," Nature Photon. **4**, 557–560 (2010).
42. O. Boyraz, T. Indukuri, and B. Jalali, "Self-phase-modulation induced spectral broadening in silicon waveguides," Opt. Express **12**, 829–833 (2004).
43. I-W. Hsieh, X. Chen, X. Liu, J. I. Dadap, N. C. Panoiu, C.-Y. Chou, F. Xia, W. M. Green, Y. A. Vlasov, and R. M. Osgood, Jr., "Supercontinuum generation in silicon photonic wires," Opt. Express **15**, 15242–15249 (2007).
44. F. Leo, S. Gorza, J. Safioui, P. Kockaert, S. Coen, U. Dave, B. Kuyken, and G. Roelkens, "Dispersive wave emission and supercontinuum generation in a silicon wire waveguide pumped around the 1550 nm telecommunication wavelength," Opt. Lett. **39**, 3623–3625 (2014).
45. L. Yin, Q. Lin, G. P. Agrawal, "Soliton fission and supercontinuum generation in silicon waveguides," Opt. Lett.

32, 391–393 (2007).

46. M. Zhu, H. Liu, X. Li, N. Huang, Q. Sun, J. Wen, and Z. Wang, "Ultrabroadband flat dispersion tailoring of dual-slot silicon waveguides," Opt. Express **20**, 15899–15907 (2012).
47. L. Zhang, Q. Lin, Y. Yue, Y. Yan, R. G. Beausoleil, and A. E. Willner, "Silicon waveguide with four zero-dispersion wavelengths and its application in on-chip octave-spanning supercontinuum generation," Opt. Express **20**, 1685–1690 (2012).
48. L. Zhang, Q. Lin, Y. Yue, Y. Yan, R. G. Beausoleil, A. Agarwal, L. C. Kimerling, J. Michel, and A. E. Willner, "On-chip octave-spanning supercontinuum in nanostructured silicon waveguides using ultralow pulse energy," IEEE J. Sel. Topics Quantum Electron. **18**, 1799–1806 (2012).
49. C. Bao, Y. Yan, L. Zhang, Y. Yue, N. Ahmed, A. M. Agarwal, L. C. Kimerling, J. Michel, and A. E. Willner, "Increased bandwidth with flattened and low dispersion in a horizontal double-slot silicon waveguide," J. Opt. Soc. Am. B **32**, 26–30 (2015).
50. R. M. Corless, G. H. Gonnet, D. E. G. Hare, D. J. Jeffrey, and D. E. Knuth, "On the Lambert *W* function," Adv. Comput. Math. **5**, 329–359 (1996).
51. V. P. Tzolov, M. Fontaine, N. Godbout and S. Lacroix, "Nonlinear self-phase-modulation effects: a vectorial first-order perturbation approach," Opt. Lett. **20**, 456–458 (1995).
52. S. Afshar V. and T. M. Monro, "A full vectorial model for pulse propagation in emerging waveguides with subwavelength structures. Part I: Kerr nonlinearity," Opt Express **17**, 2298–2318 (2009).
53. B. Tatian, "Fitting refractive-index data with the Sellmeier dispersion formula," Appl. Opt. **23**, 4477–4485 (1984).
54. D. Castelló-Lurbe, E. Silvestre, P. Andrés, and V. Torres-Company, "Spectral broadening enhancement in silicon waveguides through pulse shaping," Opt. Lett. **37**, 2757–2759 (2012).
55. J. Dudley and S. Coen, "Coherence properties of supercontinuum spectra generated in photonic crystal and tapered optical fibers," Opt. Lett. **27**, 1180–1182 (2002).
56. L. Cohen, *Time-Frequency Analysis* (Prentice Hall, 1995).
57. D. Marcuse, "Pulse distortion in single-mode fibers. 3: Chirped pulses," Appl. Opt. **20**, 3573–3579 (1981).

1. Introduction

Narrow-band pulses can suffer huge spectral broadening when they propagate throughout non-linear media due to the interplay of many nonlinear processes. It corresponds to the so-called supercontinuum (SC) generation and it finds several applications in high-precision frequency metrology [1], optical coherence tomography [2] or in telecommunications [3]. Its dynamics is highly sensitive to the physical parameters of the nonlinear system. Since photonic crystal fibers (PCF) allowed to improve the control of these properties, SC generation experienced a great development from the advent of this kind of fiber [4].

Usually, SC is generated through higher-order-soliton compression and fission and the subsequent dispersive waves (DW) emission due to the efficient spectral broadening achieved in this solitonic regime [4, 5]. Nevertheless, noise amplification produced by modulation instability (MI) can notably reduce the coherence of this SC if the soliton number of the input pulses is not kept at low enough values [4, 6]. Furthermore, even when this condition is fulfilled, there may still be a significant timing and amplitude jitter in the output pulses [7]. The impact of input pulse fluctuations can be avoided by pumping in the normal dispersion regime, where MI is not produced. In addition, the impact of the initial pulse jitter is also reduced in normally dispersive fibers [8]. However, narrower spectra are often expected under these conditions [9].

In a nonsolitonic regime, *i.e.*, if the input pulse is pumped at normal dispersion, new frequencies are generated through self-phase modulation (SPM) at the first stages of the propagation. Even an octave-spanning SC can be obtained based on this mechanism, but a flattened and low dispersion profile and high nonlinearities are required [10, 11]. However, since red-shifted frequencies move faster and blue-shifted frequencies move slower than frequencies around the carrier in the normal dispersion regime, a space-time overlapping among frequencies in the pulse tails can take place when frequencies disperse. This overlap can give rise to the so-called optical wave-breaking (OWB). Furthermore, it can favor new nonlinear interactions generating new frequencies. This phenomenon was early studied both numerically and experimentally in fibers [12–14] and recently numerically in silicon waveguides [15]. In the last years, it has been used to induce additional spectral broadening [9, 11] and for pulse compression [16]. In these

cases, it is usually studied in all-normal dispersion systems. Despite these succesfull applications, the efficiency of the spectral broadening is limited since phase-matching is not achieved in all-normal dispersion regime.

Recently, DW emission induced during OWB has been experimentally demonstrated [17] and theoretically analyzed [18, 19]. In this paper, our first goal is to study this process from a new theoretical approach [20] based on global properties of the pulse and its spectrum. That allows us to identify the nonlinear process that emit the DW and so derive analytical expressions that provide a third-order dispersion (TOD) enabling the phenomenon and the frequency of the DW without solving the nonlinear propagation equation. It is worth noting that this nonlinear process differs from the mechanism that allows solitons to emit DWs [18]. This fact is consistent with recent papers [17, 19].

Going one step further, we will apply this new strategy to produce SC in silicon-on-insulator (SOI) waveguides due to its interest for all-optical on-chip signal processing [21]. SC generation can get particular benefit from the strong third-order nonlinear optical effects [22–24] enhanced by a tight optical confinement associated to its high-index-contrast [25]. However, and in spite of these advantages, it has been demonstrated that silicon nonlinear losses limit the spectral broadening ability of this platform, in particular at telecom wavelengths [26, 27]. For short pulses at low energies, two-photon absorption (TPA) is the dominant loss mechanism [28, 29]. We will pay special attention to this case, including these nonlinear losses in our theoretical analysis. In this way, we numerically demonstrate an enhancement of the spectral broadening produced by SPM in the presence of TPA, owing to additional nonlinear mixing induced during OWB. Particularly, our numerical results show that it is feasible to achieve an octave-bandwidth SC in a dispersion engineered SOI waveguide relying on OWB, even pumping at telecom wavelengths. Moreover, this example illustrates our nonlinear inverse engineering procedure. In a first step, nonlinear pulse propagation is tailored through the approach presented here. In a second step, a waveguide (or fiber) design where the target output spectrum is achieved can be easily found by means of our inverse dispersion engineering tool [30].

2. Supercontinuum generation relying on OWB in lossless waveguides

In this section, we present a new analytical approach to study the nonlinear pulse propagation governed by the generalized nonlinear Schrödinger equation (GNLSE) [4, 31, 32],

$$\partial_z \tilde{A}(z, \omega - \omega_0) = i\beta_p(\omega)\tilde{A}(z, \omega - \omega_0) + i\gamma_0 \mathscr{F}_{\omega_0} \left[|A(z,t)|^2 A(z,t) \right], \tag{1}$$

where ω_0 is the carrier frequency, $\beta_p(\omega) = \beta(\omega) - \beta_0 - \beta_1(\omega - \omega_0)$, $\beta(\omega)$ is the propagation constant of the mode and $\beta_k = d^k\beta/d\omega^k|_{\omega_0}$. γ_0 represents the waveguide nonlinear coefficient evaluated at ω_0 and $\mathscr{F}_{\omega_0}[f(t)] = \int_{-\infty}^{\infty} dt\, e^{i(\omega - \omega_0)t} f(t)$ is the Fourier transform centered at ω_0. We focus here on the principal physical processes. Losses will be analyzed in the next section. The complex envelope, $\tilde{A}$, is defined as

$$\tilde{\mathscr{E}}(\mathbf{x}, \omega) = \tilde{A}(z, \omega - \omega_0) \frac{\mathbf{e}(\mathbf{x}_t)}{(\int_S dS\, \hat{\mathbf{z}} \cdot (\mathbf{e}_t \times \mathbf{h}_t)/2)^{1/2}} e^{i(\beta_0 + \beta_1(\omega - \omega_0))z}, \tag{2}$$

where $\tilde{\mathscr{E}}$ is the analytic signal of the electric field — strictly speaking, Eq. (1) holds for $\omega > 0$ — [31, 32], $\mathbf{e}$ and $\mathbf{h}$ are the electric and magnetic fields of the mode evaluated at ω_0, the subindex t stands for the transverse components and $\hat{\mathbf{z}}$ is the unit vector in the z-direction. The phase of the *ansatz* in Eq. (2) includes $\beta_1(\omega - \omega_0)z$, that is equivalent to moving in the time reference frame $T = t - \beta_1 z$ [33]. In addition, $\mathbf{e}_t$ and $\mathbf{h}_t$ have been selected real and $\tilde{A}$ has been normalized such that $|A(z,t)|^2$ represents the instantaneous power. The domain of the integral, S, corresponds to the transverse plane to the waveguide. Our approach is based on the following z-dependent
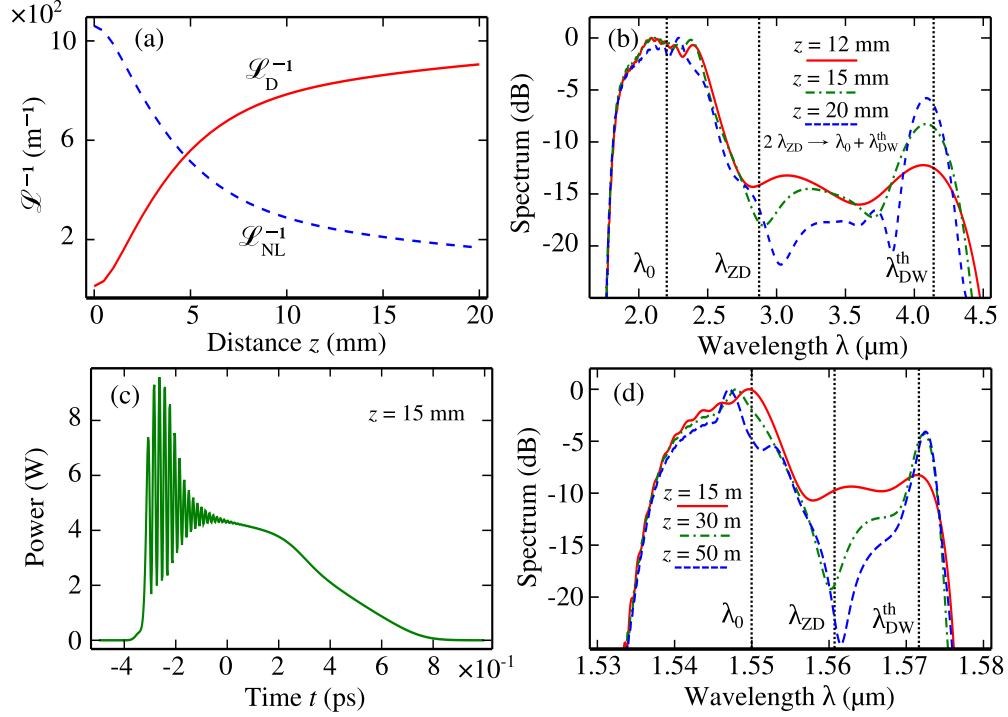
Fig. 1. (a) Evolution of the generalized lengths, $\mathscr{L}^{-1}$, in the OWB regime. It corresponds to the pulse propagation of (b-c). (b) Output spectrum for a femtosecond pulse in a waveguide. λ_0 indicates the pumping wavelength, λ_{ZD} points out the zero-dispersion wavelength [note it is the pump wave considered in Eq. (7)], and λ_{DW}^{th} refers to the theoretical wavelengths of the dispersive wave (*i.e.* the idler wave). (c) Output pulse corresponding to (b). (d) Output spectrum for a picosecond pulse in a fiber. (See text for details.)

functions,

$$\mathscr{L}_{NL}^{-1}(z) = \frac{\gamma_0 \int_{-\infty}^{\infty} dt \, |A(z,t)|^4}{2 \int_{-\infty}^{\infty} dt \, |A(z,t)|^2}, \tag{3}$$

$$\mathscr{L}_{D}^{-1}(z) = \frac{\int_{-\infty}^{\infty} d\omega \, \beta_p(\omega)|A(z,\omega-\omega_0)|^2}{\int_{-\infty}^{\infty} d\omega \, |A(z,\omega-\omega_0)|^2}. \tag{4}$$

In [20], we proposed these functions and argue that they define the length scales where SPM and the group-velocity dispersion (GVD) act at each propagation distance. In addition, the conservation law associated to the Hamiltonian of the GNLSE [34, 35] can also be expressed as $\mathscr{L}_{NL}^{-1}(z) + \mathscr{L}_{D}^{-1}(z) = \mathscr{L}_{NL}^{-1}(0) + \mathscr{L}_{D}^{-1}(0)$ [20]. Throughout the next lines, we aim at getting useful insight about the pulse propagation by analyzing the evolution of $\mathscr{L}_{D}^{-1}$ and $\mathscr{L}_{NL}^{-1}$.

Figure 1(a) illustrates the behavior of $\mathscr{L}_{D}^{-1}$ and $\mathscr{L}_{NL}^{-1}$ in a regime where OWB appears [20]. The system is characterized at the beginning by a strong nonlinearity and a positive value of the dispersive length ($\mathscr{L}_{NL}^{-1}(0) \gg \mathscr{L}_{D}^{-1}(0) > 0$), and the pulse propagation presents a monotonic increase of $\mathscr{L}_{D}^{-1}$ and, correspondingly, decrease of $\mathscr{L}_{NL}^{-1}$. It allows to identify two stages in the evolution. In the first one, $\mathscr{L}_{NL}^{-1} > \mathscr{L}_{D}^{-1}$ indicates that SPM rules the spectral broadening. In the second stage, $\mathscr{L}_{D}^{-1} > \mathscr{L}_{NL}^{-1}$ points out that new frequency generation relies on nonlinear processes mainly governed by dispersive effects. It is also worth remind-
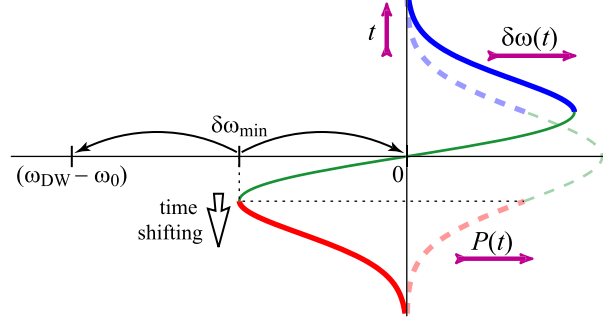
Fig. 2. Sketch for the interpretation of the FWM processes considered in this paper. We assume that the schematic plots of the instantaneous frequency, $\delta\omega(t)$ — continuous lines —, and instantaneous power, $P(t)$ — dashed lines —, correspond to the distance z_{OWB} given by Eq. (5). Thick lines highlight the blue shift and red shifht frequencies that overlap after z_{OWB}. The process described by Eq. (7) and the time shifting induced by dispersion are also represented.

ing that the fundamental nonlinear process described by Eq. (1) is four-wave mixing (FWM), $\omega_{p,1} + \omega_{p,2} \rightarrow \omega_s + \omega_i$ [31], where the subindex p,s,i refer to pump, signal and idler, respectively, and its frequency conversion efficiency depends on both linear (dispersive) and nonlinear contributions. In [20], we related the spectral broadening at this second step to the nonlinear interactions enabled during OWB. So, we defined the distance at which the second stage begins, $\mathscr{L}_D^{-1}(z_{OWB}) = \mathscr{L}_{NL}^{-1}(z_{OWB})$, as the OWB distance. In that work, we restricted our numerical study to all-normal dispersion waveguides. Nevertheless, the dynamics of the characteristic lengths suggests that only $\mathscr{L}_D^{-1} > 0$ must be satisfied in this regime and thus, an all-normal dispersion is not necessary. As a result, nonlinear processes could be on phase-matching in the second stage [36].

To test the feasibility of this scenario, we analyze FWM processes enabled in the OWB regime in the framework of the above sketched two step model.

Considering that SPM rules the pulse propagation along the first stage, and that this step ends when $\mathscr{L}_D^{-1}(z_{OWB}) \approx \frac{1}{2}\mathscr{L}_{NL}^{-1}(0)$, we can estimate the OWB distance,

$$z_{OWB} \approx \sqrt{\frac{L_D L_{NL}}{\varkappa^2 \sigma_2}}, \tag{5}$$

and the spectral content at that position — quantified by the chirp induced previously by SPM,

$$\delta\omega(z_{OWB}, t) \approx -\varkappa\gamma_0 \partial_t |A(0,t)|^2 z_{OWB}. \tag{6}$$

In the above equations, $\varkappa = (\text{arcsinh}\sqrt{3})/\sqrt{3}$, $L_{NL} = 1/(\gamma_0 P_0)$, $L_D = T_0^2/\beta_2$, and $\sigma_2 = \int_{-\infty}^{\infty} d\tau \, (\partial_\tau U_p)^2 U_p / \int_{-\infty}^{\infty} d\tau \, U_p^2$, where we have introduced a time scale normalized to the input pulse width T_0 as $\tau = t/T_0$, and a normalized power distribution U_p as $|A(0,\tau)|^2 = P_0 U_p(\tau)$; P_0 is the input pulse peak power (see Appendix A).

Among the FWM processes favored due to the space-time overlapping induced by frequency dispersion [9, 11] and the difference between their instantaneous powers in this second stage, see [20], we focus here on the degenerate FWM in which the frequency corresponding to the minimum value of the SPM-induced chirp, $\omega_0 + \delta\omega_{min}$, acts as the pump wave to generate a signal wave of frequency ω_0 and an idler wave ω_{DW},

$$2(\omega_0 + \delta\omega_{min}) \rightarrow \omega_0 + \omega_{DW}. \tag{7}$$

It is worth emphasizing two features about the above process. On the one hand, the pump wave is expected to have enough power to be transferred to the idler wave. (Note that Eq. (6) estimates a frequency range with significant powers.) On the other hand, this process can produce the minimum frequency that is attainable within this set of interactions, $\omega_{DW} - \omega_0 = 2\delta\omega_{min}$ (see Fig. 2).

The minimum frequency generated at the first stage can be written as $\delta\omega_{min} = -\varkappa\Upsilon z_{OWB}/(L_{NL}T_0)$, where Υ is the minimum value of $\partial_\tau U_p$ (see Eq. (6) and text below it). If the conventional phase-matching condition (namely, in the continuous-wave regime under the pump undepleted approximation [36]) is imposed on the process represented in Eq. (7), and neglecting the nonlinear contribution (note $\mathscr{L}_D^{-1} > \mathscr{L}_{NL}^{-1}$), then $\Delta k \equiv \beta(\omega_i) + \beta(\omega_s) - 2\beta(\omega_p) = 0$, that can be rewritten as $\Delta k = 2\sum_k \beta_{2k}(\omega_p)(\omega_s - \omega_p)^{2k}/(2k)!$ [37], where $\beta_{2k}(\omega_p) = \mathrm{d}^{2k}\beta/\mathrm{d}\omega^{2k}|_{\omega_p}$. Now, if higher order dispersion coefficients are not considered, then $\beta_2(\omega_0 + \delta\omega_{min}) = \beta_2 + \beta_3\delta\omega_{min} = 0$. That leads to

$$\beta_3 = \sqrt{\frac{\sigma_2}{\Upsilon^2}\beta_2^3 L_{NL}}, \tag{8}$$

$$\omega_{DW} - \omega_0 = \frac{-2\beta_2}{\beta_3}. \tag{9}$$

Equation (8) characterizes an scenario where the efficiency of the process depicted in Eq. (7) is optimum and, therefore, an important spectral broadening at significant power levels is expected. So, other FWM enabled in this regime will experience smaller gain, if any. In addition, Eq. (9) can be considered an estimate of the bandwidth of the output spectrum. From this point of view, these equations will also be useful for inverse engineering purposes.

It is worth comparing Eq. (9) with the frequency for the DW emitted by solitons, $\omega_{DW} - \omega_0 = -3\beta_2/\beta_3$ [38]. For the soliton case, the location of the DW was firstly derived by means of a phase-matching condition between the soliton — a nonlinear state — and the DW — a linear state — [38]. Recently, in [18], Erkintalo *et al.* demonstrated that DWs are emitted through cascaded FWM in a soliton-like propagation. Of course, the original expression for the frequency of the DW is recovered if this physical description is used. Notwithstanding, Webb *et al.* demonstrated in [17] that the frequency spreading had to be considered, unlike the solitonic regime, to explain the emission of (generalized) DW by pulses pumped in the normal dispersion regime, $\beta_2 > 0$. This case has been analyzed in [19] by Conforti and Trillo through phase-matching between a shock wave — which is, in this case, the nonlinear state — and the DW. This approach allows them to interpret different scenarios that can appear if $\beta_2 > 0$, thus providing a valuable insight even in complex regimes [39]. However, the phase-matching condition depends on the shock wave velocity, which in general can only be determined numerically [19, 39]. Here, we keep in mind design purposes, so a complete knowlegde of the complex envelope is not necessary in our framework. Instead of solving Eq. (1), as in [19, 39], we take advantage of our generalized lengths, $\mathscr{L}_{NL}^{-1}$ and $\mathscr{L}_D^{-1}$, to characterize nonlinear pulse propagation. Furthermore, it allows us to identify a particular scenario, depicted by Eq. (8) and Fig. 1(a), where DW emission is essentially due to one FWM process, see Eq. (7). Consequently, an analysis based on the fundamental nonlinear process (that also explains the origin of the DW radiated by the shock wave in this scenario) can be driven. Moreover, it leads to an analytical expression for the frequency of the DW [see Eq. (9)], which turns out very useful to design waveguides for SC generation.

Finally, it should be taken into account that our free parameters, namely γ_0, β_2 and $A(0,t)$, must entail that $\mathscr{L}_{NL}^{-1}(0) \gg \mathscr{L}_D^{-1}(0) > 0$ [9, 20, 40]. In addition, the β_3 predicted by Eq. (8) must not distort the wave-breaking regime represented in Fig. 1(a). Under such conditions we

can select and favor one of the possible four-wave mixing processes as it has been mentioned. Other cases beyond the scope of this work will be studied elsewhere.

Now, we test Eqs. (8) and (9) by solving numerically Eq. (1). In Fig. 1(b), a Gaussian pulse of 150 fs full-width at half-maximum (FWHM) in amplitude and 30 W of peak power propagates throughout a 20 mm-long waveguide with $\gamma_0 = 100\,\mathrm{W^{-1}m^{-1}}$ and $\beta_2 = 0.2\,\mathrm{ps^2m^{-1}}$. These parameters are feasible in silicon waveguides pumped at $2.2\,\mu\mathrm{m}$ [41]. Equations (8) and (9) indicate $\beta_3 = 0.001\,\mathrm{ps^3m^{-1}}$ and $\lambda_{\mathrm{DW}} = 4.129\,\mu\mathrm{m}$ for these values. The solid curve in Fig. 1(b) corresponds to the output spectrum in this case and it is in excellent agreement with our model. On the one hand, the evolution of $\mathscr{L}_{\mathrm{NL}}^{-1}$ and $\mathscr{L}_{\mathrm{D}}^{-1}$ is not notably modified when our theoretical β_3 is considered, though efficient new frequency generation is enabled. In other words, the behavior shown in Fig. 1(a) is similar to that observed when only β_2 controls dispersive effects (see [20]). On the other hand, a resonance is observed at the theoretical position of the DW emitted according to our model. In Fig. 1(d), a Gaussian pulse of $T_{\mathrm{FWHM}} = 1\,\mathrm{ps}$, 300 W of peak power, propagates throughout a 50 m-long (commercially available) fiber with $\gamma_0 = 4\,\mathrm{W^{-1}km^{-1}}$, $\beta_2 = 25\,\mathrm{ps^2km^{-1}}$. In this case, Eq. (8) provides $\beta_3 = 3\,\mathrm{ps^3km^{-1}}$ and Eq. (8), $\lambda_{\mathrm{DW}} = 1.572\,\mu\mathrm{m}$. The solid curve in Fig. 1(d) is also in accordance with our theoretical results. This indicates that this scenario can appear regardless of the input pulse duration, provided that suitable dispersion could be attained.

3. Supercontinuum generation relying on OWB in the presence of TPA

Usually SC generation pumping in the normal dispersion regime is based on SPM [10, 11]. It requires high nonlinearities. So, SOI waveguides could be an excellent platform to accomplish this goal. Nevertheless, TPA coefficient of silicon increases dramatically below $2.2\,\mu\mathrm{m}$, being very relevant at telecom wavelengths [22–24]. Consequently, the spectral broadening produced by SPM quickly saturates in SOI waveguides when pumped in the near infrared (IR) [26,42,43].

SC generation has already been studied both numerically and experimentally in silicon waveguides [44–48]. These works exploit pulse propagation in the solitonic regime, *i.e.*, input pulses are pumped at the anomalous dispersion regime. Here we explore SC generation in silicon waveguides, but in the wave-breaking regime, even pumping at telecom wavelengths.

In Section 2 we have confirmed that new frequency generation in the wave-breaking regime can be analyzed in two stages. Certainly, the nonlinear processes considered in the second stage only depends on the frequencies created in the first stage. From this point of view, the broadening mechanism of the first stage is not crucial, provided that frequency dispersion continues governed by β_2. Therefore, the presence of TPA does not invalidate our approach for these cases. In particular, we can deal with TPA by means of the *effective* nonlinear coefficient, $\hat{\gamma}_0$, of an equivalent lossless waveguide producing, at $\hat{z}_{\mathrm{OWB}}$, the same minimum chirp that is generated in the waveguide affected by TPA at the same distance. Attending to [26,45], and ignoring dispersive effects in the first stage in both equivalent systems,

$$\min_t \{\delta\omega^{\mathrm{TPA}}(t,\hat{z}_{\mathrm{OWB}})\} = \min_{\hat{t}} \{\delta\hat{\omega}(\hat{t},\hat{z}_{\mathrm{OWB}})\},$$

$$\min_t \left\{ \frac{-\mathrm{Re}(\gamma_0)\partial_t|A(0,t)|^2\,\hat{z}_{\mathrm{OWB}}}{1+2\,\mathrm{Im}(\gamma_0)|A(0,t)|^2\,\hat{z}_{\mathrm{OWB}}} \right\} = -\hat{\gamma}_0 \min_{\hat{t}} \left\{ \partial_{\hat{t}}|A(0,\hat{t})|^2 \right\} \hat{z}_{\mathrm{OWB}}, \tag{10}$$

where $\hat{z}_{\mathrm{OWB}} = \sqrt{L_{\mathrm{D}}\hat{L}_{\mathrm{NL}}/(\varkappa^2\sigma_2)}$ [*cf.* Eq. (5)], $\hat{L}_{\mathrm{NL}} = 1/(\hat{\gamma}_0 P_0)$, and $\hat{\gamma}_0$ is a real quantity — in contrast to γ_0, that is complex when TPA is considered [26].

If a Gaussian pulse is considered, Eq. (10) can be developed to derive
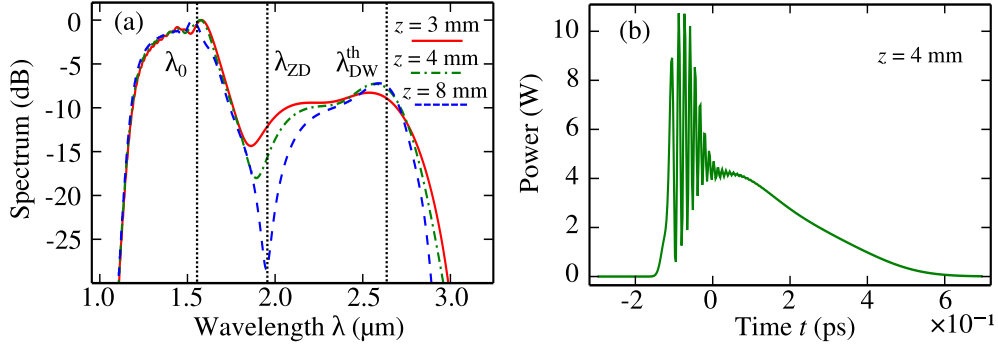
$$W^2 - 2\zeta^2 W - \zeta^2 = 0, \tag{11}$$

Fig. 3. (a) Output spectra produced by OWB and SPM in the presence of TPA (see details in the text). (b) Output pulse corresponding to the solid curve spectrum in (a).

where $\zeta = e^{-1/2} \left[\text{Im}(\gamma_0)/\text{Re}(\gamma_0) \right] (\hat{z}_{\text{OWB}}/\hat{L}_{\text{NL}})$, $W = W_0 \left[e^{-1/2} \text{Im}(\gamma_0) P_0 \hat{z}_{\text{OWB}} \right]$, being W_0 the Lambert function [50]. For hyperbolic secant pulses, the corresponding equation is

$$\frac{\text{Re}(\gamma_0)}{\hat{\gamma}_0} = \frac{4}{3\sqrt{3}} \frac{\sqrt{1-x}}{x^2}, \tag{12}$$

where $x = 4/(3 + \sqrt{9 + 16\,\text{Im}(\gamma_0)\,P_0\,\hat{z}_{\text{OWB}}})$.

In Fig. 3(a), a Gaussian input pulse with $T_{\text{FWHM}} = 50\,\text{fs}$, analogously to [45], and 300 W of peak power is propagated throughout a 8 mm-long waveguide with $\gamma_0 = (100 + 10i)\,\text{W}^{-1}\text{m}^{-1}$, $\beta_2 = 0.2\,\text{ps}^2\text{m}^{-1}$ and $\beta_3 = 8 \times 10^{-4}\,\text{ps}^3\text{m}^{-1}$. This value for β_3 is obtained by means of Eq. (8) when the effective nonlinearity calculated through Eq. (11), $\hat{\gamma}_0 = 29\,\text{W}^{-1}\text{m}^{-1}$, is considered. The spectrum after some propagation distances appears in Fig. 3(a). This case shares common features with Figs. 1(b) and 1(d). On the one side, a sidelobe close to $\lambda_{\text{DW}} = 2.634\,\mu\text{m}$, that corresponds to the theoretical value given by Eq. (8), is observed. On the other side, similarly to Fig. 1(c), the output pulse shows temporal oscillations at the leading pulse edge. It indicates that this spectral broadening occurs during OWB, in agreement with our modelling. Despite TPA losses, the spectral broadening produced SPM gets the zero-dispersion wavelength. Moreover, neither β_3 nor TPA disturb in this case the frequency overlapping in the pulse tails induced by β_2. This keeps our reasoning valid even for significant nonlinear losses.

Up to now, we have tested our analytical tools in some ideal cases. It has provided a significant insight about the main processes involved in SC generation in silicon waveguides pumping in the normal dispersion regime. In the next section, we take advantage of these conclusions to simulate a realistic propagation in a properly engineered silicon waveguide.

4. Inverse design of a silicon waveguide

The objective of this section is to find a silicon waveguide design where an octave spanning SC generation relying on OWB can be demonstrated. The analytical results presented in this paper allows us to fix γ_0, β_2, β_3 without intensive trial-and-error procedures. Indeed the parameters obtained in the previous section can be used as targets in an inverse engineering approach, according to [30]. We apply this strategy here and propose a silicon waveguide for SC generation. Its geometry, dispersion and nonlinear coefficient curves are plotted in Figs. 4(a) and 4(b).

For the sake of completeness we include free-carrier related processes using an extended version of the GNLSE to simulate the pulse propagation,

$$\partial_z \tilde{A} = -\frac{\alpha}{2}\tilde{A} + i\beta_p(\omega)\tilde{A} + i\gamma(\omega)\mathscr{F}_{\omega_0}\left[|A|^2 A\right] - \frac{\sigma}{2}(1 + i\mu)\mathscr{F}_{\omega_0}\left[N_c(z,t)A\right], \tag{13}$$
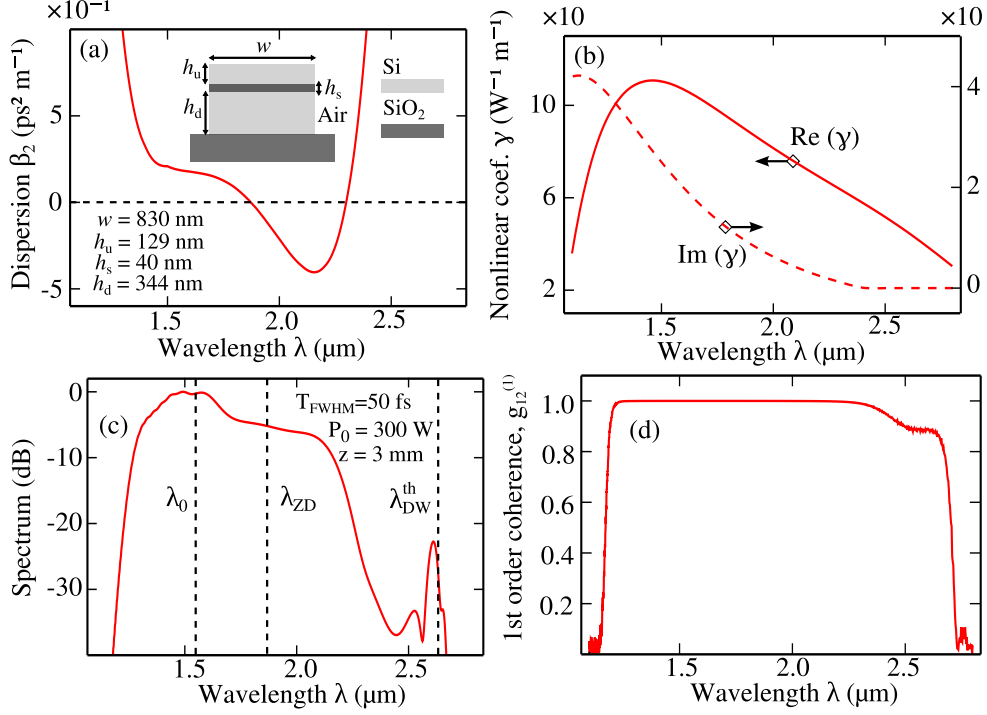
Fig. 4. (a) Dispersion curve of a strip silicon waveguide with a slot of SiO_2 [47] (included as an inset). (b) Complex nonlinear coefficient. (c) Output spectrum spanning an octave after a propagation distance of 3 mm. (d) Modulus of the complex degree of first order coherence corresponding to (c)
.

$$N_c(z,t) = \frac{2\pi \left[\text{Im}(\gamma_0)\right]^2}{h\omega_0\beta_{\text{TPA}}(\omega_0)} \int_{-\infty}^{t} e^{-\frac{t-t'}{\tau_c}} |A(z,t')|^4 dt', \tag{14}$$

where α corresponding to 7 dB/cm [47] takes into account linear losses, h is the Planck constant, $\sigma = 1.45 \times 10^{-21}$ m^2 is the FCA coefficient, $\mu = 7.5$ represents the relative weight of FCD, and $\tau_c = 1$ ns is the carrier lifetime [28, 29, 45]. In addition, we calculate the nonlinear coefficient, including both material and mode dispersion, according to the following expression [51, 52]:

$$\gamma(\omega) = \frac{\varepsilon_0}{\mu_0(\int_S (\mathbf{e}_t \times \mathbf{h}_t) \cdot \hat{\mathbf{z}} dS)^2} \int_S dS \left[\frac{\omega n_2}{c} + i\frac{\beta_{\text{TPA}}}{2}\right] \rho n^2 \left[(\mathbf{e}_t \cdot \mathbf{e}_t)^2 + \frac{2}{3}\mathbf{e}_t \cdot \mathbf{e}_t |e_z|^2 + |e_z|^4\right], \tag{15}$$

where ε_0 is the vacuum permittivity, and μ_0 is the vacuum permeability. We attend to the experimental data from [23, 24] to characterize the dispersion of the Kerr index, n_2, and the TPA coefficient, β_{TPA}, of silicon (see Appendix B) and take $n_2 = 2.6 \times 10^{-20}$ m^2 W^{-1} for silica [36]. The parameter ρ characterizes the nonlinear anisotropy. We consider $\rho = 1.27$ for silicon [28] and $\rho = 1$ for silica. Note that frequency and transverse coordinates dependence of the integrand has been omitted in Eq. (15). Following [52], we ignore the term that accounts for polarization effects in the nonlinear phenomena for silicon waveguides [28]. In addition, Sellmeier coefficients of the refractive index, n, of silicon and silica were taken from [53].

In Fig. 4(c) we consider a propagation supported by the fundamental TM mode of a slotted silicon waveguide [47–49], see inset in Fig. 4(a). (Note that Raman scattering can be safely

neglected for such a mode [28, 47, 48]). It gives rise to an octave-spanning SC generation when a Gaussian pulse with $T_{\text{FWHM}} = 50\,\text{fs}$ and $P_0 = 300\,\text{W}$ is propagated $3\,\text{mm}$ throughout the waveguide. A dispersive wave is emitted close to $\lambda_{\text{DW}} = 2.634\,\mu\text{m}$, in spite of the higher order terms of both the group-velocity dispersion and the nonlinear coefficient [*cf.* Fig. 3(a)]. It agrees with the dispersive wave emitted through the nonlinear process considered in our approach. [Note that $\Delta k = \beta_2(\omega_p)(\omega_s - \omega_p)^2 + 1/12\,\beta_4(\omega_p)(\omega_s - \omega_p)^4 + ...$, so the phase-mismatch is still quite controlled by $\beta_2(\omega_p)$ when higher order dispersion is considered. Equation (19) could be used to deal with these higher-order effects.]

The difference on the efficiency of the DW emission compared to Fig. 3(a) can be mainly atributed to the dispersion of both real and imaginary parts of the nonlinear coefficient. It is worthwhile to note that similar results can be obtained for lower peak powers if asymmetric input pulses are used [54]. Finally, we have computed the complex degree of first order coherence attending to [55] in Fig. 4(d). We simulated input pulse fluctuations including one photon per mode with a random phase and averaged over 1000 realizations. It confirms that highly stable SC generation is achieved in the wave-breaking regime.

5.   Conclusions

A new approach to deal with nonlinear pulse propagation based on the evolution of two average magnitudes of pulses has been presented in this work. They allow characterizing the dynamical regime and identify the most important physical processes at work. Analytical expressions to delimit the different stages in the SC generation as well as suitable dispersion curves to stimulate certain nonlinear processes have been derived. It represents an advance compared to the usual "brute-force" design strategies. Interestingly, these results indicate that key features of the pulse evolution can be determined even when complete information about the pulse at each propagation distance is not available. Our approach makes easier the design tasks of SC sources. By applying this nonlinear inverse engineering, we easily find a design of a silicon waveguide where an octave-spanning SC can be produced pumping at telecom wavelengths in the normal dispersion regime. We emphasize that the huge spectral broadening relies here on nonlinear processes enabled during wave-breaking, unlike common SC produced in a solitonic regime.

Appendix A

In this appendix we outline the derivation of Eqs. (5) and (6). For the sake of completeness, we also indicate how higher-order dispersion can be taken into account when z_{OWB} is derived.

Firstly, starting from the Taylor expansion of $\beta_p(\omega)$, we can rewrite $\mathscr{L}_{\text{D}}^{-1}(z) = \sum_{k=2}(\beta_k/k!)\mu_k(z)$, where μ_k is the kth moment of the spectrum at the baseband. Since the action of SPM is straightforward in the time domain, it is convenient to calculate μ_k in that domain. It can be done, attending to [56], as

$$\mu_k = \frac{\int_{-\infty}^{\infty} d\omega\,(\omega - \omega_0)^k |\tilde{A}(\omega - \omega_0)|^2}{\int_{-\infty}^{\infty} d\omega\,|\tilde{A}(\omega - \omega_0)|^2} = \frac{\int_{-\infty}^{\infty} dt\,A^*(t)(i\partial_t)^k A(t)}{\int_{-\infty}^{\infty} dt\,|A(t)|^2} \approx \frac{\int_{-\infty}^{\infty} dt\,[-\partial\varphi(t)]^k |A(t)|^2}{\int_{-\infty}^{\infty} dt\,|A(t)|^2},$$

(16)

where we only retain the contribution of the envelope phase, φ, being $A(t) = |A(t)|e^{i\varphi(t)}$ and $\tilde{A}(\omega - \omega_0) = \int_{-\infty}^{\infty} dt\, e^{i(\omega - \omega_0)t} A(t)$. In order to evaluate $\partial_t \varphi$, we take into account dispersion through the following ansatz [57]:

$$|A(z,t)|^2 = a(z) \left| A\left(0, \frac{t}{\sqrt{1+\alpha z^2}}\right) \right|^2. \tag{17}$$

From the energy conservation of the pulse and the condition $\mathscr{L}_D^{-1}(z_{\mathrm{OWB}}) \approx \mathscr{L}_{\mathrm{NL}}^{-1}(0)/2$, we derive $a(z) = (1+\alpha z^2)^{-1/2}$ and $\alpha = 3/z_{\mathrm{OWB}}^2$. It allows us to calculate the instantaneous frequency distribution at z_{OWB}, Eq. (6),

$$\delta\omega(z_{\mathrm{OWB}},t) = -\partial_t \varphi(z_{\mathrm{OWB}},t) \approx -\gamma_0 \int_0^{z_{\mathrm{OWB}}} dz\, \partial_t |A(z,t)|^2 \approx -\varkappa \gamma_0 \partial_t |A(0,t)|^2 z_{\mathrm{OWB}}, \tag{18}$$

where $\varkappa = (\mathrm{arcsinh}\sqrt{3})/\sqrt{3}$.

Equation (5) can be generalized to include higher-order dispersion provided $\beta_p(\omega)$ is a symmetric function with respect to ω_0. Following the procedure presented in Section 2, we can derive

$$\sum_{k=2} \frac{(-1)^k}{k!} \frac{L_{\mathrm{NL}}}{L_D^{(k)}} \left(\frac{\varkappa z_{\mathrm{OWB}}}{L_{\mathrm{NL}}} \right)^k \sigma_k = \frac{1}{2}, \tag{19}$$

where $L_D^{(k)} = T_0^k/\beta_k$ and $\sigma_k = \int_{-\infty}^{\infty} d\tau\, (\partial_\tau U_p)^k U_p / \int_{-\infty}^{\infty} d\tau\, U_p^2$. Equation (19) is in agreement with the numerical results shown in Fig. 1 in [20]. We want to emphasize that this equation allows us to evaluate the impact of higher-order dispersion on z_{OWB} with no additional efforts, unlike previous approaches based on approximate solutions of the pulse profile [9, 40].

Appendix B

For the convenience of the reader, we have included in this appendix the numerical fit considered in Section 4 to describe the dispersion of the Kerr index, n_2, and the TPA coefficient, β_{TPA}, of silicon. We have fitted the experimental measurements presented in [23, 24] to a Cauchy model of the form $\sum_{k=0}^{2} a_k/\lambda^{2k}$. The parameters a_k are included in Table 1. The mean values of such fits has been employed to evaluate the nonlinear coefficient [see Eq. (15)] within the range of interest.

Table 1. Cauchy parameters for the Kerr index and the two-photon absorption coefficient.

Magnitude (*units*)	a_0 (*units*)	a_1 (*units* $\times \mu\mathrm{m}^2$)	a_2 (*units* $\times \mu\mathrm{m}^4$)
n_2 $(\mathrm{m}^2\mathrm{W}^{-1})$ [23]	-9.31422×10^{-19}	1.78924×10^{-17}	-2.25824×10^{-17}
β_{TPA} $(\mathrm{m\,W}^{-1})$ [23]	-8.03605×10^{-12}	5.07515×10^{-11}	-4.63796×10^{-11}
n_2 $(\mathrm{m}^2\mathrm{W}^{-1})$ [24]	1.83568×10^{-17}	-3.49209×10^{-17}	2.02215×10^{-17}
β_{TPA} $(\mathrm{m\,W}^{-1})$ [24]	-9.18175×10^{-12}	6.22685×10^{-11}	-3.11114×10^{-11}